Modelling shear lag phenomenon for adhesively bonded piezo - transducers

Suresh Bhalla and Ashok Gupta
Department of Civil Engineering, Indian Institute of Technology Delhi, Hauz Khas,
New Delhi 110016, India

1. Introduction

During the last one and a half decades, the electro-mechanical impedance (EMI) technique has emerged as a universal cost-effective technique for structural health monitoring (SHM) and non destructive evaluation (NDE) of all types of engineering structures and systems (Sun et al., 1995; Ayres et al., 1998; Soh et al., 2000; Park et al., 2000, 2001; Giurgiutiu and Zagrai, 2000, 2002; Bhalla & Soh, 2003, 2004a, 2004b, 2004c). In this technique, a lead zirconate titanate piezo-electric ceramic (PZT) patch, surface bonded to the monitored structure, employs ultrasonic vibrations (typically in 30-400 kHz range), to derive a characteristic electrical 'signature' of the structure (in frequency domain), containing vital information concerning the phenomenological nature of the structure. Electro-mechanical admittance, which is the measured electrical parameter, can be decomposed and analyzed to extract the mechanical impedance parameters of the host structure (Bhalla & Soh, 2004b, 2004c). In this manner, the PZT patch, acting as 'piezo-impedance transducer', enables structural identification, health monitoring and NDE (Bhalla, 2004).

The PZT patches are made up of 'piezoelectric' materials, which generate surface charges in response to mechanical stresses and conversely undergo mechanical deformations in response to electric fields. In the EMI technique, the bonded PZT patch is electrically excited by applying an alternating voltage using an impedance analyzer. This produces deformations in the patch as well as in the local area of the host structure surrounding it. The response of this area is transferred back to the PZT wafer in the form of admittance (the electrical response), comprising of the conductance (the real part) and the susceptance (the imaginary part). Hence, the same PZT patch acts as an actuator as well as a sensor concurrently. Any damage to the structure manifests itself as a deviation in the admittance signature, which serves as an indication of the damage (assuming that the integrity of the PZT patch is granted).

The EMI technique has been shown to possess far greater sensitivity to structural damages than the conventional global vibration techniques. It is typically of the order of the local ultrasonic techniques. The EMI technique employs low-cost PZT patches, which can be permanently bonded to the structures and unlike the ultrasonic techniques, can be interrogated without removal of the finishes or rendering the monitored structure out of service. In addition, no complex data processing or expensive hardware is warranted since

the data is directly acquired in frequency domain. The limited sensing area of the piezo-impedance transducers helps in isolating the effects of far field changes, such as mass loading and normal operational vibrations, thereby enabling damage localization (Park et al., 2000).

The PZT patches are normally bonded to the surface of the monitored component using adhesives, which introduce the so-called 'shear lag effect'. This chapter is primarily focused on development of analytical models for considering the shear lag effect inherent in the adhesively bonded PZT patches for direct use in SHM/ NDE via the EMI technique. The chapter covers a review of the modelling strategies since the 1980s and presents a detailed description of two shear lag models specifically developed for the EMI technique, the first one by Bhalla & Soh in 2004 and the second one, a simplified version, by Bhalla, Kumar, Gupta and Datta in 2009.

2. Impedance Modelling of PZT-structure Interaction

The PZT patches, which play the key role in the EMI technique, typically develop surface charges under mechanical stresses; and conversely undergo mechanical deformations when subjected to electric fields, expressed mathematically by (IEEE standard, 1987)

$$D_i = \overline{\varepsilon_{ij}^T} E_j + d_{im} T_m \tag{1}$$

$$S_k = d_{jk} E_j + \overline{s_{km}^E} T_m \tag{2}$$

where D_i is the electric displacement, S_k the mechanical strain, E_j the electric field and T_m the mechanical stress. $\overline{\varepsilon_{ij}^T}$ denotes the complex electric permittivity of the PZT material at constant stress, d_{im} and d_{jk} the piezoelectric strain coefficients (or constants) and $\overline{s_{km}^E}$ the complex elastic compliance at constant electric field. The superscripts 'T' and 'E' indicate that the quantity has been measured at constant stress and constant electric field respectively.

During the last one and half decades, several attempts have been made to model the PZT-structure electromechanical interaction. The beginning was made by Crawley and de Luis (1987) in the form of 'static approach', later substituted by the 'impedance approach' of Liang, et al. (1994). Liang and coworkers modelled the host structure as mechanical impedance Z_s connected to the PZT patch at the end, as shown in Fig. 1(a), with the patch undergoing axial vibrations under an alternating electric field E_3. Mathematically, Z_s is related to the force F and the velocity $\dot{u}$ by

$$F_{(x=l)} = -Z_S \dot{u}_{(x=l)} \tag{3}$$

Solution of the governing 1D wave Eq. resulted in following expression for the complex electromechanical admittance for the system of Fig. 1(a)
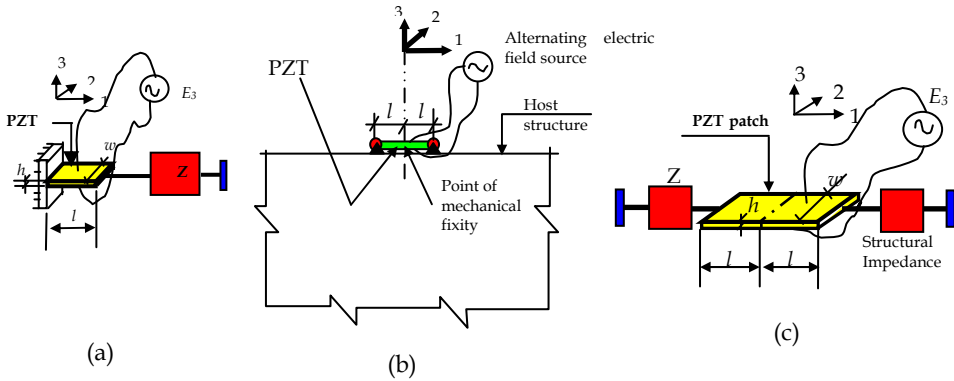
Fig. 1. (a) Liang's 1D impedance model (Liang et al. 1994).
(b) A PZT patch surface-bonded to a structure.
(c) Impedance model for the system shown in (b).

$$\overline{Y} = G + Bj = \omega j \frac{wl}{h} \left[(\overline{\varepsilon_{33}^{T}} - d_{31}^{2} \overline{Y^{E}}) + \left(\frac{Z_a}{Z_S + Z_a} \right) d_{31}^{2} \overline{Y^{E}} \left(\frac{\tan \kappa l}{\kappa l} \right) \right] \tag{4}$$

where w, l and h represent the PZT patch's dimensions (see Fig. 1a), d_{31} the piezoelectric strain coefficient for the 1-3 axes and ω the angular frequency. $\overline{Y^{E}} = Y^{E}(1 + \eta j)$ is the complex Young's modulus of the PZT patch (at constant electric field) and $\overline{\varepsilon_{33}^{E}} = \varepsilon_{33}^{E}(1 - \delta j)$ the complex electric permittivity (at constant stress), with the symbols η and δ denoting the mechanical loss factor and the dielectric loss factor respectively. Z_a represents the mechanical impedance of the PZT patch (in short circuited condition), given by

$$Z_a = \frac{\kappa wh}{\tan \kappa l} \frac{\overline{Y^{E}}}{(j\omega)} \tag{5}$$

where κ, the wave number, is related to the density ρ and the Young's modulus $\overline{Y^{E}}$ of the patch by

$$\kappa = \omega \sqrt{\frac{\rho}{\overline{Y^{E}}}} \tag{6}$$

In real-life applications, where the PZT patch is surface-bonded on a structure, as shown in Fig. 1(b), the nodal plane passes through the centre line of the patch. The structure can be represented as a set of two impedances Z_s connected on the either side of the patch, as illustrated in Fig. 1(c). For this scenario, l would be the half-length of the patch and Eq. (4) needs to be modified as

$$\overline{Y} = G + Bj = 2\omega j \frac{wl}{h} \left[(\overline{\varepsilon_{33}^{T}} - d_{31}^{2} \overline{Y^{E}}) + \left(\frac{Z_a}{Z_S + Z_a} \right) d_{31}^{2} \overline{Y^{E}} \left(\frac{\tan \kappa l}{\kappa l} \right) \right] \tag{7}$$

Zhou et al. (1996) extended the formulations of Liang to model the a PZT element coupled to a 2D host structure. The related physical model is schematically illustrated in Fig. 2. Zhou and coworkers replaced the single term Z_s by a matrix consisting of the direct impedances Z_{xx} and Z_{yy}, and the cross impedances Z_{xy} and Z_{yx}, related to the planar forces F_1 and F_2 (along axes 1 and 2 respectively) and the corresponding planar velocities $\dot{u}_1$ and $\dot{u}_2$ by

$$\begin{bmatrix} F_1 \\ F_2 \end{bmatrix} = -\begin{bmatrix} Z_{xx} & Z_{xy} \\ Z_{yx} & Z_{yy} \end{bmatrix}\begin{bmatrix} \dot{u}_1 \\ \dot{u}_2 \end{bmatrix} \tag{8}$$

Considering dynamic equilibrium along the two principal axes in conjunction with piezoelectric constitutive relations (Eqs. 1 and 2), they derived

$$\overline{Y} = j\omega \frac{wl}{h}\left[\varepsilon_{33}^T - \frac{2d_{31}^2 \overline{Y^E}}{(1-\nu)} + \frac{d_{31}^2 \overline{Y^E}}{(1-\nu)}\left\{ \frac{\sin \kappa d}{l} \quad \frac{\sin \kappa w}{w}\right\}\left\{ \begin{matrix} \kappa\cos(\kappa l)\left\{1 - \nu\frac{w}{l}\frac{Z_{xy}}{Z_{axx}} + \frac{Z_{xx}}{Z_{axx}}\right\} & \kappa\cos(\kappa w)\left\{\frac{l}{w}\frac{Z_{yx}}{Z_{ayy}} - \nu\frac{Z_{yy}}{Z_{ayy}}\right\} \\ \kappa\cos(\kappa l)\left\{\frac{w}{l}\frac{Z_{xy}}{Z_{axx}} - \nu\frac{Z_{xx}}{Z_{axx}}\right\} & \kappa\cos(\kappa w)\left\{1 - \nu\frac{l}{w}\frac{Z_{yx}}{Z_{ayy}} + \frac{Z_{yy}}{Z_{ayy}}\right\} \end{matrix} \right\}^{-1}\left\{ \begin{matrix} 1 \\ 1 \end{matrix} \right\} \right] \tag{9}$$

where κ, the 2D wave number, is given by

$$\kappa = \omega\sqrt{\frac{\rho(1-\nu^2)}{\overline{Y^E}}} \tag{10}$$

Z_{axx} and Z_{ayy} are the two components of the mechanical impedance of the PZT patch along the two principal directions, given by Eq. 5. Although the analytical derivations of Zhou and co-workers are accurate in themselves, the experimental difficulties prohibit their direct application for the inverse problem, i.e. the extraction of host structure's mechanical impedance. Using the EMI technique, one can experimentally obtain two parameters- G and B for a surface-bonded PZT patch. If complete information about the structure is desired, Eq. (9) needs to be solved for 4 complex unknowns- Z_{xx}, Z_{yy}, Z_{xy}, Z_{yx} (or 8 real unknowns). Hence, the model could not be employed for the experimental determination of the drive point mechanical impedance from measurements alone.

To alleviate these shortcomings, the concept of 'effective impedance' was introduced by Bhalla & Soh (2004b). The related physical model is shown in Fig. 3 for a square-shaped PZT patch of half-length l. Bhalla & Soh (2004b) represented the PZT-structure interaction in the form of boundary traction f per unit length, varying harmonically with time. The 'effecive mechanical impedance', $Z_{a,eff}$, of the patch was defined as
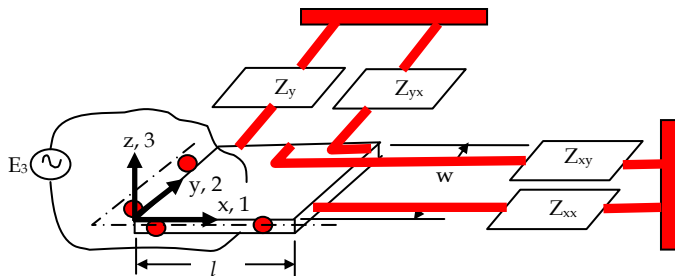

Fig. 2. 2D impedance model of Zhou et al. (1996).

$$Z_{a,eff} = \frac{F_{eff}}{\dot{u}_{eff}} = \frac{\oint_S \vec{f}.\hat{n}\,ds}{\dot{u}_{eff}} = \frac{2h\overline{Y^E}}{j\omega(1-\nu)\overline{T}} \qquad (11)$$

where F_{eff} is the overall planar force (or the effective force) causing area deformation of the PZT patch and $\hat{n}$ the unit vector normal to the boundary. $u_{eff} = \delta A/p_o$ is the 'effective displacement', with δA denoting the change in the patch's area and p_o its original undeformed perimeter. Differentiation of the effective displacement with respect to time yields the effective velocity, $\dot{u}_{eff}$. The effective drive point impedance of the host structure can be similarly defined, by applying a force on the surface of the host structure, along the boundary of the proposed location of the PZT patch. The term $\overline{T}$ is the complex tangent ratio, theoretically equal to [$tan(\kappa l)/\kappa l$]. However, in actual situations, it needs correction to realistically consider the deviation of the PZT patch from the ideal behavior, to accommodate which Bhalla and Soh (2004b) introduced correction factors as

$$\overline{T} = \frac{1}{2}\left(\frac{\tan C_1 \kappa l}{C_1 \kappa l} + \frac{\tan C_2 \kappa l}{C_2 \kappa l} \right) \qquad (12)$$

The correction factors C_1 and C_2 can be determined from the experimentally obtained conductance and susceptance signatures of the PZT patch in 'free-free' conditions before bonding it on the host structure. It has been demonstrated that this 'updating' enables much more accurate reults. Solution of the governing 2D wave Eq. for this system yielded following expression for the complex electro-mechanical admittance $\overline{Y}$

$$\overline{Y} = G + Bj = 4\omega \ j\frac{l^2}{h}\left[\overline{\varepsilon_{33}^T} - \frac{2d_{31}^2\overline{Y^E}}{(1-\nu)} + \frac{2d_{31}^2\overline{Y^E}}{(1-\nu)}\left(\frac{Z_{a,eff}}{Z_{s,eff} + Z_{a,eff}} \right)\overline{T} \right] \qquad (13)$$
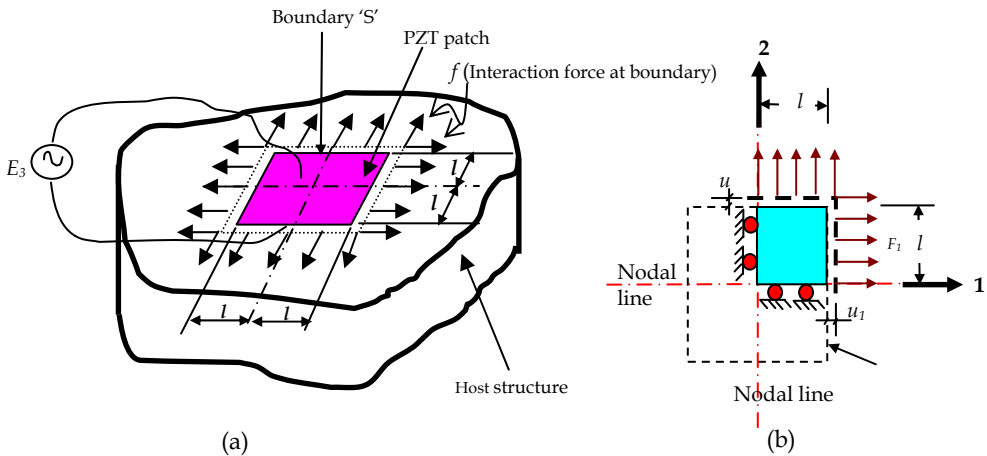

Fig. 3. Effective impedance model of Bhalla & Soh (2004a).
(a) PZT bonded to host structure. (b) Interaction forces at boundary.

Here, a single complex term for $Z_{s,eff}$ (rather than four terms as in Zhou's model) accounts for the 2D mechanical interaction of the patch with the host structure. This makes the resulting equation. simple enough to solve the inverse problem, i.e. to extract $Z_{s,eff}$ (Bhalla & Soh, 2004c), to be directly utilized for SHM/ NDE. No modelling is required for the host structure and the necessary data is directly obtainable from experimental measurements. Further, the corrected actuator effective impedance, $Z_{a,eff}$, can be expressed as

$$Z_{a,eff} = \frac{2h\overline{Y^E}}{j\omega(1-\nu)\overline{\overline{T}}} \tag{14}$$

All the above models ignore the fact that the mechanical interaction between the PZT patch and the host structure occurs through a finitely thick layer of adhesive sandwiched between the PZT patch and the host structure, which introduces the so-called 'shear lag effect' through its elastic deformation. Presented in the following sections is a detailed review of the shear lag mechanism inherent in adhesively bonded PZT patches and its rigorous integration in 1D and 2D impedance models, as proposed by Bhalla & Soh (2004d). Further, a new simplified model model proposed by Bhalla et al. (2009), which is especially suitable for solving the inverse problem (of extracting Z_s), considering the presence of bond layer, is also described.

3. Shear Lag Effect

Crawley and de Luis (1987) and Sirohi and Chopra (2000) respectively modelled the actuation and sensing of a generic beam element by an adhesively bonded PZT patch. The typical configuration of the system is shown in Fig. 4. The patch has a half-length l, width w_p and thickness h_p, while the bonding layer has a thickness h_s. The beam has depth h_b and width w_b. Let T_p be the axial stress in the PZT patch and τ the interfacial shear stress. The system is under quasi-static equilibrium and the beam is actuated in pure bending mode, with the bending strain linearly distributed across the cross section. Further, the PZT patch is in a state of pure 1D axial strain and the bond layer in pure shear, with the shear stress independent of 'y'. The ends of the segmented PZT actuator/ sensor are stress free, implying a uniform strain distribution across the thickness of the patch. A more detailed deformation profile is shown in Fig. 5 for the symmetrical right half of the system. Let u_p be the displacement at the interface between the PZT patch and the bond layer, and u the corresponding displacement at the interface between the bond layer and the beam. The following subsections briefly review the shear transfer mechanism for sensor and actuator respectively.

3.1 PZT patch as sensor
Let the PZT patch be instrumented only to sense the strain on the beam surface, and hence, no external electric field be applied across it. Considering static equilibrium of the differential element of the PZT patch in the x-direction, as shown in Fig. 4, we can derive

$$\tau = \frac{\partial T_p}{\partial x} h_p \tag{15}$$

At any cross section of the beam, within the portion containing the PZT patch, the bending moment is given by

$$M = T_p w_p h_p (0.5h_b + h_S + 0.5h_p) \tag{16}$$

Using Euler-Bernoulli's beam theory and assuming $(h_p + 2h_s) << h_b$, we can reduce Eq. (16) to

$$T_b + \left(\frac{3T_p w_P h_p}{w_b h_b} \right) = 0 \tag{17}$$

where T_b denotes the bending stress on the beam surface. Differentiating with respect to x, and substituting Eq. (15), we get

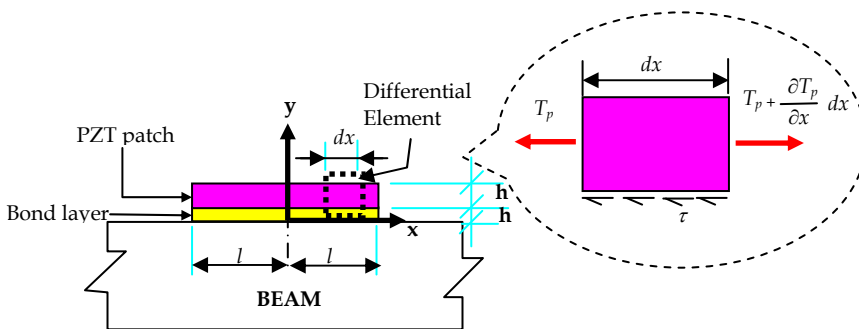$$\frac{\partial T_b}{\partial x} + \left(\frac{3w_P}{w_b h_b} \right) \tau = 0 \tag{18}$$

Fig. 4. A PZT patch bonded to a beam using adhesive bond layer.

Further, substituting $T_b = Y_b S_b$, $T_p = Y^E S_p$ and $\tau = G_s \gamma = G_s (u_p - u)/u$ into Eq.s (15) and (18), and differentiating with respect to x, we respectively obtain
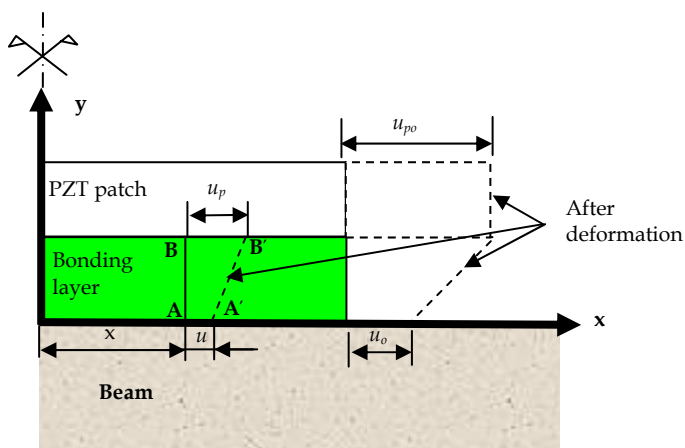

Fig. 5. Deformation in bonding layer and PZT patch.

$$\frac{\partial^2 S_P}{\partial x^2} = \left(\frac{G_s S_b}{Y_P h_S h_P}\right)\xi \qquad (19)$$

$$\frac{\partial^2 S_b}{\partial x^2} = -\left(\frac{3w_P G_s S_b}{Y_b w_b h_b h_P}\right)\xi \qquad (20)$$

where Y_b is the Young's modulus of elasticity of the beam, S_b and S_P the beam and PZT strains, G_s the shear modulus of the bond layer, γ the shear strain in the bond layer and $\xi = (S_p / S_b - 1)$. Subtracting Eq. (20) from Eq. (19), we get

$$\frac{\partial^2 \xi}{\partial x^2} - \Gamma^2 \xi = 0 \qquad (21)$$

Where
$$\Gamma^2 = \left(\frac{G_s}{Y_P h_s h_P} + \frac{3G_s w_P}{Y_b w_b h_b h_P}\right) \qquad (22)$$

This phenomenon of the difference in the PZT strain and the host structure's strain is called the *shear lag effect*. The parameter Γ (unit m-1) is called the *shear lag parameter*. The ratio ξ, which is a measure of the differential PZT strain relative to surface strain of the host substrate, is called the *strain lag ratio*. The general solution for Eq. (21) is

$$\xi = A\cosh\Gamma x + B\sinh\Gamma x \qquad (23)$$

Since no external electric field is applied across the PZT patch, the free PZT strain, $d_{31}E_3 = 0$. Thus, at $x = -l$, $S_P = 0 \Rightarrow \xi = -1$. Similarly, at $x = +l$, $\xi = -1$. Applying these boundary conditions, we can obtain

$$\xi = -\frac{\cosh(\Gamma x)}{\cosh(\Gamma l)} \qquad (24)$$

Since
$$\xi = (S_p / S_b - 1),$$

$$\frac{S_P}{S_b} = \left[1 - \frac{\cosh(\Gamma x)}{\cosh(\Gamma l)}\right] \qquad (25)$$

Fig. 6 shows a plot of the strain ratio (S_P/S_b) across the length of a PZT patch (l = 5mm) for typical values of Γ = 10, 20, 30, 40, 50 and 60 (cm-1). It is observed that the strain ratio (S_P/S_b) is less than unity near the ends of the PZT patch. The length of this zone depends on Γ, which in turn depends on the stiffness and thickness of the bond layer (Eq. 22). As G_s increases and h_s reduces, Γ increases, the shear lag phenomenon diminishes and the shear is effectively transferred over very small zones near the ends of the PZT patch.
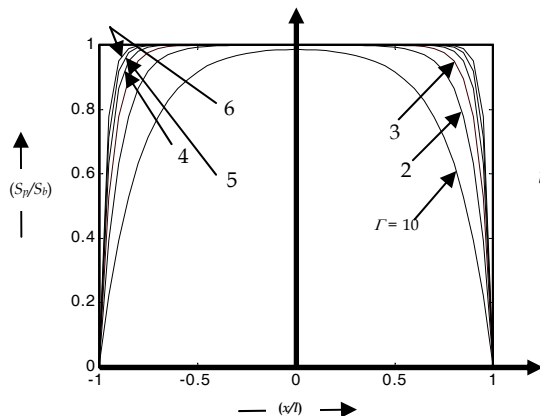
Fig. 6. Strain distribution across the length of PZT patch for various values of Γ.
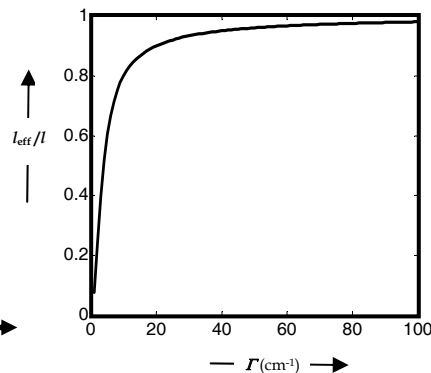
Fig. 7. Variation of effective length with shear lag factor.

This analysis shows that if the PZT patch is employed as a sensor, it would develop less voltage across its terminals (than for perfectly bonded conditions) and hence underestimate the strain in the substructure. In order to quantify the effect of shear lag, we can compute the effective length, l_{eff}, of the sensor, as defined by (Sirohi and Chopra, 2000)

$$\frac{l_{eff}}{l} = \frac{1}{l}\int_{x=0}^{x=l}(S_p / S_b)dx = 1 - \frac{\tanh(\Gamma l)}{\Gamma l} \tag{26}$$

which is nothing but the area under the curve (Fig. 6) between $x/l = 0$ and $x/l = 1$. Fig. 7 shows a plot of the effective length (Eq. 26) for various values of the shear lag parameter Γ. From this figure, it can be observed that typically, for $\Gamma > 30\text{cm}^{-1}$, ($l_{eff} / l$) is very large, typically greater than 93%, suggesting that shear lag effect can be ignored for relatively high (> 30 cm^{-1}) values of Γ.

3.2 PZT patch as actuator
If the same PZT patch is employed as an actuator for a beam structure, it can be shown (Crawley and de Luis, 1987) that the strains S_P and S_b are given by

$$S_p = \frac{3\Lambda}{(3+\psi)} + \frac{\Lambda\psi\cosh\Gamma x}{(3+\psi)\cosh\Gamma l} \quad \text{and} \quad S_b = \frac{3\Lambda}{(3+\psi)} - \frac{3\Lambda\cosh\Gamma x}{(3+\psi)\cosh\Gamma l} \tag{27}$$

where $\Lambda = d_{31}E_3$ is the free piezoelectric strain, and $\psi = (Y_b h_b/Y^E h_p)$ the product of modulus and thickness ratios of the beam and the PZT patch. Fig. 8 shows the plots of (S_p/Λ) and (S_b/Λ) along the length of the PZT patch (l = 5mm) for ψ = 15. It is observed that as in the case of sensor, as Γ increases, the shear is effectively transferred over small zone near the two ends of the patch. Typically, for $\Gamma > 30\text{cm}^{-1}$, the strain energy induced in the substructure by PZT actuator is within 5% of the perfectly bonded case.
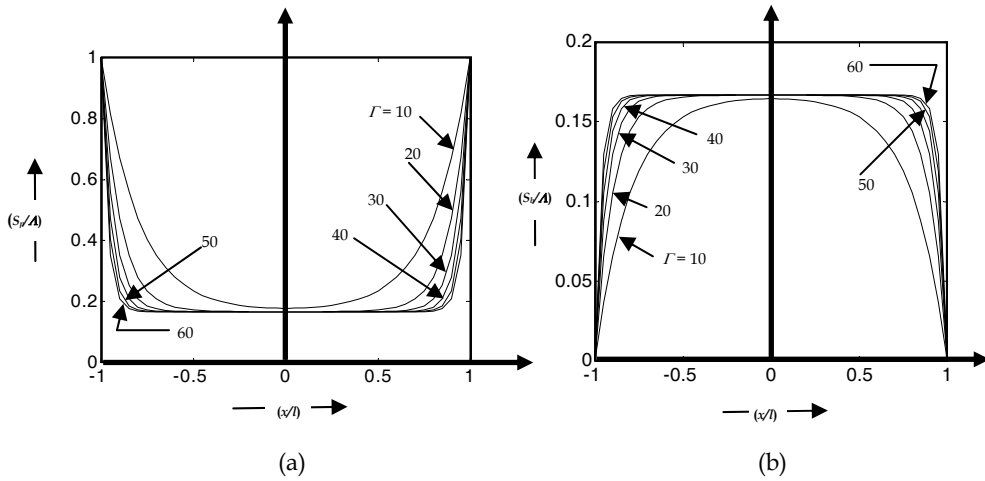
(a)   (b)

Fig. 8. Distribution of piezoelectric and beam strains for various values of Γ.
(a) Strain in PZT patch. (b) Beam surface strain.

4. Shear Lag Effect in Electro-Mechanical Impedance Formulations

It is observed in the preceding section that when acting as an actuator and/ or a sensor, there is shear lag phenomenon associated with force transmission between the PZT patch and the host structure through the adhesive bond layer. However, this aspect has not been thoroughly investigated for the EMI technique, in which the same patch concurrently serves both as a sensor as well as an actuator. Abe et al. (2002) encountered large errors in their stress prediction methodology using EMI technique, which were attributed to imprecise modeling of the interfacial bonding layer. This highlights the importance of modelling the shear lag mechanism accurately.

Xu and Liu (2002) proposed a modified 1D impedance model in which the bonding layer was modelled as a single degree of freedom (SDOF) system connected in between the PZT patch and the host structure, as shown in Fig. 9. The bonding layer was assumed to possess a dynamic stiffness $\overline{K_b}$ (or mechanical impedance, $Z_b = \overline{K_b}/j\omega$) and the structure a dynamic stiffness $\overline{K_S}$ (or mechanical impedance, $Z_s = \overline{K_S}/j\omega$). Hence, the resultant mechanical impedance for this series system can be determined as (Hixon, 1988)

$$Z_{res} = \frac{Z_b Z_s}{Z_b + Z_s} = \left(\frac{\overline{K_b}}{\overline{K_b} + \overline{K_S}} \right) Z_s = \zeta Z_S \tag{28}$$

where

$$\zeta = \frac{1}{1 + \left(\overline{K_S} / \overline{K_b} \right)} \tag{29}$$

The coupled electromechanical admittance, as measured across the terminals of the PZT patch and expressed earlier by Eq. (4), can therefore be modified as

$$\overline{Y} = 2\omega j \frac{wl}{h} \left[(\overline{\varepsilon_{33}^T} - d_{31}^2 \overline{Y^E}) + \left(\frac{Z_a}{Z_a + \zeta Z_s} \right) d_{31}^2 \overline{Y^E} \left(\frac{\tan \kappa l}{\kappa l} \right) \right] \qquad (30)$$

$\zeta = 1$ implies infinitely stiff bond layer where as $\zeta = 0$ implies a free PZT patch. Xu and Liu (2002) demonstrated numerically that for a SDOF system, as ζ decreases (i.e. as the bond quality degrades), the PZT system shows an increase in the associated structural resonant frequencies. It was stated that $\overline{K_b}$ depends on the bonding process and the thickness of the bond layer. However, no closed form solution was presented to quantitatively determine $\overline{K_b}$ and hence ζ (From Eq. 29). Also, no experimental verification was attempted.

Ong et al. (2002) integrated the shear lag effect into impedance modelling using the analysis presented by Sirohi and Chopra (2000). The PZT patch was assumed to possess an effective length l_{eff} (Eq. 26) instead of the actual length. However, since the effective length was determined by considering sensor effect only, the method considered the associated shear lag only partially. Also, the resulting formulations are valid for beam type structures only and are not generic in nature. In addition, since frequencies of the order of 30-400 kHz are involved in the EMI technique, quasi-static approximation (for calculating l_{eff}) is strictly not valid. The next section presents the model of Bhalla & Soh (2004d) to alleviate all the above shortcomings.

5. Rigorous Shear Lag Model (Bhalla & Soh, 2004d)

5.1 1D shear lag model
This section presents a detailed step-by-step analysis for including the shear lag effect, first into 1D model (Liang et al., 1994) and then its extension into 2D effective impedance based model (Bhalla & Soh, 2004b).
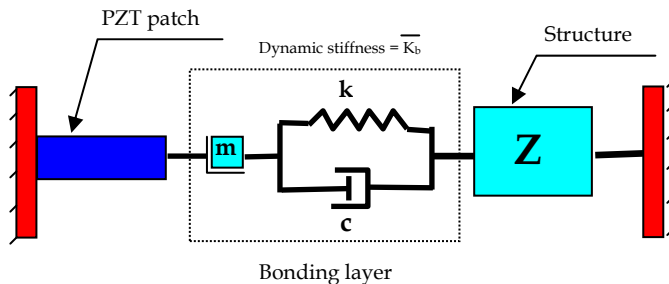

Fig. 9. Modified impedance model of Xu and Liu (2002) including bond layer.

Consider the PZT patch, shown in Figs. 4 and 5, to be driven by an alternating voltage source and let it be attached to any host structure (not necessarily beam). Also, we assume the PZT patch to be infinitesimally small as compared to the host structure. This means that the host structure has constant mechanical impedance all along the points of attachment of the patch. By D'Alembert's principle, the dynamic equilibrium of an infinitesimal element of the patch leads to

$$\tau w_p dx + (dm)\frac{\partial^2 u_p}{\partial t^2} = \frac{\partial T_p}{\partial x} h_p w_p dx \tag{31}$$

where dm is the infinitesimal mass of the element considered. Due to the dominance of the shear stress term, the inertial term can be neglected, which reduces Eq. (31) to Eq. (15). It should be noted that the inertial force term has been separately considered in impedance formulations (Liang et al., 1994), where, as a matter of fact, the shear lag effect has been ignored. Hence, the two effects are independently considered and will be finally combined. Assuming pure shear in the bond layer,

$$\tau = \frac{\overline{G_s}(u_p - u)}{h_s} \tag{32}$$

where $\overline{G_s} = G_s(1 + \eta' j)$ is the complex shear modulus of the bond layer and η' is the associated mechanical loss factor. From PZT constitutive relation, Eq. (2), the axial stress in the PZT patch is given by

$$T_p = \overline{Y^E}(S_p - \wedge) = \overline{Y^E}(u'_p - \wedge) \tag{33}$$

where $S_p = u'_p$ is the PZT strain and $\wedge = E_3 d_{31}$ is the free piezoelectric strain. Substituting Eq.s (32) and (33) into Eq. (15) and simplifying, we get

$$u_p - u = \left(\frac{\overline{Y^E} h_p h_s}{\overline{G_s}} \right) u''_p \tag{34}$$

At any vertical section through the host structure (which includes the PZT patch), the force transmitted to the host structure is related to the drive point impedance Z_s of the host structure by

$$F = T_p w_p h_p = -Z_s u j \omega \tag{35}$$

where u is the drive point displacement at the point in question on the surface of the host structure. Since the PZT patch is infinitesimally small, Z_s is practically the same along the entire length of the PZT patch. Substituting Eq. (33), differentiating with respect to x (noting that Z_s is constant), and rearranging, we get

$$u''_p = -\left(\frac{Z_s j \omega}{w_p h_p \overline{Y^E}} \right) u' \tag{36}$$

From Eq.s (34) and (36), we derive

$$u_p - u = -\left(\frac{Z_s h_s j \omega}{G_s w_p} \right) u' \tag{37}$$

Eq.s (34) and (37) are the fundamental Eq.s governing the shear transfer mechanism via the adhesive bonding layer. Eliminating u_p from these equations and differentiating with respect to x, we can derive

$$u''' + \bar{p}u''' - qu'' = 0 \tag{38}$$

where

$$\bar{p} = -\frac{w_p \bar{G_s}}{Z_s h_s j\omega} \tag{39}$$

and

$$q = \frac{\bar{G_s}}{Y^E h_s h_p} = \frac{G_s(1 + \eta' j)}{Y^E h_s h_p (1 + \eta j)} \approx \frac{G_s}{Y^E h_s h_p} \tag{40}$$

$\bar{p}$ and q are shear lag parameters, similar to the factor Γ in Eq. (22). The parameter q is equivalent to the first component of Γ and $\bar{p}$ to the second component. As seen from Eq. (40), q is directly proportional to the bond layer's shear modulus and inversely proportional to the PZT patch's Young's modulus, the PZT patch's thickness and the bond layer thickness. Examination of Eq. (39) similarly shows that $\bar{p}$ is directly proportional to the bond layer's shear modulus and the PZT patch's width. It is inversely proportional to structural mechanical impedance and the bond layer thickness. Being dynamic parameter, the frequency ω also comes into picture, influencing $\bar{p}$ inversely. Further, it should be noted that $\bar{p}$ is a complex term whereas the term q is approximated as a pure real term assuming η and η' to be very small in magnitude. Solving Eq. (41), we get the roots of the characteristic Eq. as

$$\lambda_1 = 0, \quad \lambda_2 = 0, \quad \lambda_3 = \frac{-\bar{p} + \sqrt{\bar{p}^2 + 4q}}{2}, \quad \lambda_4 = \frac{-\bar{p} - \sqrt{\bar{p}^2 + 4q}}{2} \tag{41}$$

Hence, the solution of the governing differential equation (Eq. 38) can be written as

$$u = A_1 + A_2 x + B e^{\lambda_3 x} + C e^{\lambda_4 x} \tag{42}$$

Differentiating with respect to x, we get

$$u' = A_2 + B\lambda_3 e^{\lambda_3 x} + C\lambda_4 e^{\lambda_4 x} \tag{43}$$

From Eqs (37), (42) and (43), we obtain

$$u_p = (A_1 + \bar{n}A_2) + A_2 x + B(1 + \bar{n}\lambda_3)e^{\lambda_3 x} + C(1 + \bar{n}\lambda_4)e^{\lambda_4 x} \tag{44}$$

where
$$\bar{n} = \left(-\frac{\bar{Z}h_s j\omega}{w_p \bar{G_s}} \right) \tag{45}$$

Differentiating Eq. (44) with respect to x, we obtain the strain in the PZT patch as

$$S_p = A_2 + B\lambda_3(1+\bar{n}\lambda_3)e^{\lambda_3 x} + C\lambda_4(1+\bar{n}\lambda_4)e^{\lambda_4 x} \tag{46}$$

At $x = 0$ (see Figs 4 and 5), $u = 0$, hence Eq. (42) leads to

$$A_1 = -(B + C) \tag{47}$$

Similarly, applying the boundary condition that at $x = 0$ and $u_p = 0$ to Eq. (44) leads to

$$A_2 = -(B\lambda_3 + C\lambda_4) \tag{48}$$

Hence, Eq. (46) can be modified as

$$S_p = B[\lambda_3(1+\bar{n}\lambda_3)e^{\lambda_3 x} - \lambda_3] + C[\lambda_4(1+\bar{n}\lambda_4)e^{\lambda_4 x} - \lambda_4] \tag{49}$$

The third and the fourth boundary conditions are imposed by the stress free ends of the PZT patch. That is, at $x = -l$ and at $x = +l$, the axial strain in the PZT patch is equal to the free piezoelectric strain or $\Lambda = E_3 d_{31}$ (Crawley and de Luis, 1987). This leads to constants B and C as

$$\begin{bmatrix} B \\ C \end{bmatrix} = \frac{\Lambda}{(k_1 k_4 - k_2 k_3)} \begin{bmatrix} k_4 - k_2 \\ k_1 - k_3 \end{bmatrix} \tag{50}$$

where $\quad k_1 = \lambda_3(1+\bar{n}\lambda_3)e^{-\lambda_3 l} - \lambda_3$, $\quad k_2 = \lambda_4(1+\bar{n}\lambda_4)e^{-\lambda_4 l} - \lambda_4$, $\quad k_3 = \lambda_3(1+\bar{n}\lambda_3)e^{\lambda_3 l} - \lambda_3 \quad$ and
$k_4 = \lambda_4(1+\bar{n}\lambda_4)e^{\lambda_4 l} - \lambda_4$.

In general, the force transmitted to the host structure can be expressed as

$$F = -Z_s j\omega u_{(x=l)} \tag{51}$$

where $u_{(x=l)}$ is the displacement at the surface of the host structure at the end point of the PZT patch. Conventional impedance models (for example, Liang and coworkers) assume perfect bonding between the PZT patch and the host structure, i.e. the displacement compatibility $u_{(x=l)} = u_{p(x=l)}$, thereby approximating Eq. (51) as $F = -Z_s j\omega u_{p(x=l)}$. However, due to the shear lag phenomenon associated with finitely thick bond layer, $u_{(x=l)} \neq u_{p(x=l)}$. Based on the analysis presented in this section, we can obtain following relationship between $u_{(x=l)}$ and $u_{p(x=l}$ from Eq. (37)

$$\frac{u_{(x=l)}}{u_{p(x=l)}} = \frac{1}{1 - \left(\dfrac{Z_s h_s j\omega}{w_p \overline{G_s}}\right)\dfrac{u'_{(x=l)}}{u_{(x=l)}}} = \frac{1}{\left(1 + \dfrac{1}{\overline{p}}\dfrac{u'_o}{u_o}\right)} \tag{52}$$

The term u'_o / u_o can be determined by using Eq.s (42) and (43). Making use of this relationship, Eq. (51) can be rewritten as

$$F_S = \frac{-Z_s}{\left(1 + \dfrac{1}{\overline{p}}\dfrac{u'_o}{u_o}\right)} j\omega u_{p(x=l)} = Z_{s,eq} j\omega u_{p(x=l)} \tag{53}$$

where $Z_{s,eq} = Z_s \Big/ \left(1 + \dfrac{1}{\overline{p}}\dfrac{u'_o}{u_o}\right)$ is the 'equivalent impedance' apparent at the ends of the PZT patch, taking into consideration the shear lag phenomenon associated with the bond layer. In the absence of shear lag effect (i.e. perfect bonding), $Z_{s,eq} = Z_s$. On comparing with the result of Xu and Liu (2002) i.e. Eq. (29), we find that

$$\zeta = \frac{1}{1 + \dfrac{1}{\overline{p}}\dfrac{u'_o}{u_o}} \tag{54}$$

Hence, the derivation presented in this section enables quantitative prediction of the modifying term of the structural impedance, which was left undone by Xu and Liu (2002).

5.2 Extension to 2D shear lag model

The formulations derived above can be easily extended to the 2D effective impedance based electro-mechanical model introduced by Bhalla & Soh (2004b). For this derivation, it is assumed that the PZT is square in shape with a half-length equal to l. The strain distribution and the associated shear lag are determined along each principal direction and the two effects are assumed to be independent, which means that the effects at the corners are neglected.

The patch is assumed to be mechanically isotropic and piezoelectrically orthotropic in the x-y plane. The constitutive relations (Equations 1 and 2) can be thus reduced to (see Figure 3)

$$D_3 = \overline{\varepsilon_{33}^T} E_3 + d_{31}(T_1 + T_2) \tag{55}$$

$$S_1 = \frac{T_1 - \nu T_2}{\overline{Y^E}} + d_{31} E_3 \tag{56}$$

$$S_2 = \frac{T_2 - \nu T_1}{\overline{Y^E}} + d_{31} E_3 \tag{57}$$

Consider an infinitesimal element of the PZT patch, in dynamic equilibrium with the host structure, as shown in Fig. 10. Since this figure shows a planar view, the shear stresses τ_{xz} and τ_{yz} are not visible. Considering force equilibrium along x-direction, we can write (De Faria, 2003)

$$\frac{\partial T_1}{\partial x} + \frac{\partial \tau_{xy}}{\partial y} - \frac{\tau_{xz}}{h_p} = 0 \tag{58}$$

Ignoring the terms involving rate of change of shear strains (consistent with the observation by Zhou et al., 1996), we get
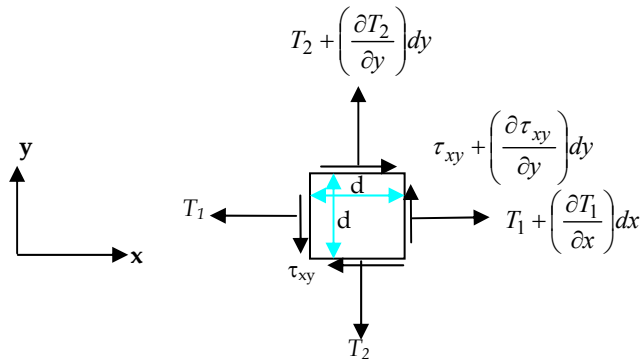

Fig. 10. Stresses acting on an infinitesimal PZT element.

$$\frac{\partial T_1}{\partial x} = \frac{\tau_{xz}}{h_p} \tag{59}$$

Further, using Eqs (56) and (57), we can derive (noting $\Lambda = E_3 d_{31}$)

$$T_1 = \frac{\overline{Y^E}}{(1 - \upsilon^2)} \left[(S_1 + \upsilon S_2) - \Lambda(1 + \nu) \right] \tag{60}$$

or

$$T_1 = \frac{\overline{Y^E}}{(1 - \upsilon^2)} \left[(u'_{px} + \upsilon u'_{py}) - \Lambda(1 + \nu) \right] \tag{61}$$

Differentiating with respect to x and ignoring the second order terms involving both x and y (Zhou et al., 1996), we get

$$\frac{\partial T_1}{\partial x} = \frac{\overline{Y^E}}{(1 - \upsilon^2)} u''_{px} \tag{62}$$

Substituting Eq. (62) into Eq. (59), expanding the term τ_{xz} and rearranging, we get

$$u_{px} - u_x = \frac{\overline{Y^E} h_s h_p}{\overline{G_s}(1-\upsilon^2)} u''_{px} \tag{63}$$

Similarly, for the other direction, we get

$$u_{py} - u_y = \frac{\overline{Y^E} h_s h_p}{\overline{G_s}(1-\upsilon^2)} u''_{py} \tag{64}$$

Adding Eqs (63) and (64) and dividing by 2, we obtain, based on the definition of 'effective displacement' that is $u_{eff} = \dfrac{\delta A}{p_o} = \dfrac{u_1 l + u_2 l + u_1 u_2}{2l} \approx \dfrac{u_1 + u_2}{2}$ (see Fig. 3), we obtain

$$u_{p,eff} - u_{eff} = \left(\frac{\overline{Y^E} h_p h_s}{\overline{G_s}(1-\upsilon^2)} \right) u''_{p,eff} \approx \frac{1}{\overline{q_{eff}}} u''_{p,eff} \tag{65}$$

where q_{eff} has been approximated as pure real number, as in the 1D case. Here, $u_{p,eff}$, by definition, is the effective displacement at the interface between the PZT patch and the bond layer, u_{eff} is the corresponding effective displacement at the interface between the structure and the bond layer. Further, from the definition of effective impedance, we can write, for the host structure

$$F = T_1 l h_p + T_2 l h_p = -Z_{s,eff} u_{eff} j\omega \tag{66}$$

Making use of Eqs. (56) and (57), and noting $\Lambda = E_3 d_{31}$, we get

$$\frac{\overline{Y^E} l h_p (S_{p1} + S_{p2} - 2\Lambda)}{(1-\upsilon)} = -Z_{s,eff} u_{eff} j\omega \tag{67}$$

Substituting for $S_{p1} = u'_{px}$, $S_{p2} = u'_{py}$, making use of the definition of effective displacement, and differentiating, we can derive

$$u''_{p,eff} = -\left[\frac{Z_{s,eff}(1-\upsilon) j\omega}{2\overline{Y^E} l h_p} \right] u'_{p,eff} \tag{68}$$

Eliminating $u''_{p,eff}$ from E.s (65) and (68), we get

$$u_{p,eff} - u_{eff} = -\left(\frac{Z_{s,eff} h_s j\omega}{2G_s(1+\upsilon)l} \right) u'_{eff} = \left(\frac{1}{\overline{p_{eff}}} \right) u'_{eff} \tag{69}$$

Thank You for previewing this eBook

You can read the full version of this eBook in different formats:

- ➢ HTML (Free /Available to everyone)

- ➢ PDF / TXT (Available to V.I.P. members. Free Standard members can access up to 5 PDF/TXT eBooks per month each month)

- ➢ Epub & Mobipocket (Exclusive to V.I.P. members)

To download this full book, simply select the format you desire below